



# Controlled synthesis of spherical $\alpha$ -Ni(OH)<sub>2</sub> hierarchical nanostructures via a simple hydrothermal process and their conversion to NiO

Masoud Salavati-Niasari<sup>a,b,\*</sup>, Maryam Entesari<sup>b</sup>

<sup>a</sup> Institute of Nano Science and Nano Technology, University of Kashan, Kashan, P.O. Box 87317-51167, Islamic Republic of Iran

<sup>b</sup> Department of Inorganic Chemistry, Faculty of Science, University of Kashan, Kashan, P.O. Box 87317-51167, Islamic Republic of Iran

## ARTICLE INFO

### Article history:

Received 25 July 2011

Accepted 22 November 2011

Available online 6 December 2011

### Keywords:

Nickel hydroxide

Nickel oxide

Chemical synthesis

Hierarchical structure

Hydrothermal

## ABSTRACT

Hierarchical pure  $\alpha$ -nickel hydroxide ( $\alpha$ -Ni(OH)<sub>2</sub>) nanostructures have been successfully synthesized through a one-step hydrothermal synthesis with nickel nitrate hexahydrate, ethylene-1,2-diamine (en) and hydrazine (N<sub>2</sub>H<sub>4</sub>) as morphology-directing agents. Optimum conditions to obtain high yield and phase pure  $\alpha$ -Ni(OH)<sub>2</sub> were identified by varying experimental parameters, such as the en and N<sub>2</sub>H<sub>4</sub> concentration, and the reaction temperature. The products were characterized by X-ray diffraction (XRD), scanning electron microscopy (SEM), transmission electron microscopy (TEM), and photoluminescence (PL) spectroscopy. For determination of the structural formula of such  $\alpha$ -nickel hydroxides, Fourier transform infrared (FT-IR) spectra and thermogravimetric analysis (TGA) were carried out on the as-prepared products. These results indicated that the  $\alpha$ -nickel hydroxide contains water molecules and anions. The hierarchical NiO nanostructures are obtained on annealing the  $\alpha$ -Ni(OH)<sub>2</sub> nanostructures at 300 °C for 4 h. The magnetic properties of the as-prepared NiO nanostructures show a superparamagnetic behavior for the as-synthesized NiO nanostructures.

© 2011 Elsevier Ltd. All rights reserved.

## 1. Introduction

Hierarchical nano/micro-structures with specific morphologies have fascinated scientists all over the world because of their sophisticated architectures, which are expected to provide some unique and exciting properties [1–3].

Nickel hydroxide is widely used in many applications, from power tools to portable electronics and electric vehicles. There are two polymorphs of nickel hydroxide, which are designated as  $\alpha$ -Ni(OH)<sub>2</sub> and  $\beta$ -Ni(OH)<sub>2</sub>, respectively. The  $\alpha$ -Ni(OH)<sub>2</sub> phase displays a more disordered and larger interlayer spacing (47.5 Å) as the interlamellar space contains anions, e.g., NO<sub>3</sub><sup>-</sup>, CO<sub>3</sub><sup>2-</sup>, SO<sub>4</sub><sup>2-</sup> and water molecules. The hexagonal  $\beta$ -Ni(OH)<sub>2</sub> phase is composed of brucite-like and well-oriented Ni(OH)<sub>2</sub> layers which are perfectly stacked along the *c*-axis with an interlamellar distance of 4.60 Å [4–6]. As an active material of the positive electrode of alkaline rechargeable batteries, the performance of such batteries highly depends on the size, morphology and phase of Ni(OH)<sub>2</sub>. Considerable work has been focused on the morphology-controllable preparation of Ni(OH)<sub>2</sub> and related composite materials [7–9].

\* Corresponding author at: Institute of Nano Science and Nano Technology, University of Kashan, Kashan, P.O. Box 87317-51167, Islamic Republic of Iran. Tel.: +98 361 591 2383; fax: +98 361 555 29 30.

E-mail address: [salavati@kashanu.ac.ir](mailto:salavati@kashanu.ac.ir) (M. Salavati-Niasari).

In view of these advantages, the synthesis of phase pure  $\alpha$ -Ni(OH)<sub>2</sub> and its stabilization in alkali solutions have attracted many researchers and mixed results have been reported. The formation of mixed phases by homogeneous precipitation of nickel salts in the presence of (NH<sub>2</sub>)<sub>2</sub>CO has been reported [10]. Delahaye-Vidal and Figiarz [11] precipitated the  $\alpha$ -phase from aqueous nickel nitrate solutions with NH<sub>3</sub> [12]. Al-substituted  $\alpha$ -Ni(OH)<sub>2</sub> was prepared by Zhao et al. [13] in the presence of surfactants such as Tween-20 and polyvinyl alcohol at 90 °C; the particles were 58–283 nm in size. Electrochemical impregnation of the  $\alpha$ -phase into sintered nickel plates was shown to be temperature dependent [14];  $\alpha$ -Ni(OH)<sub>2</sub> forms below 60 °C, but a mixed phase with nickel oxyhydroxy nitrate forms above 60 °C. The most significant work has been reported by Akine et al. [15], who hydrothermally synthesized  $\alpha$ -Ni(OH)<sub>2</sub> at 90 °C with a concentration of (NH<sub>2</sub>)<sub>2</sub>CO that was 30 times higher than that of nickel nitrate and in the presence of the dispersant HPMC (hydroxyl propyl methyl cellulose). The surface area of the particles was good with a submicrometre range size and the yield was nominal.

Nickel oxide (NiO) is an antiferromagnetic oxide semiconductor of the NaCl-type structure and is one of the most exhaustively investigated transition metal oxides. It is a promising candidate for many applications, such as battery cathodes [16], catalysis [17], gas sensors [18] and magnetic materials [19]. NiO is another material which, being a wide bandgap *p*-type semiconductor (direct gap 3.9 eV), can be employed for the fabrication of *p*–*n* heterojunctions

**Table 1**  
Experimental conditions for the preparation of Ni(OH)<sub>2</sub> and NiO nanostructures.

Sample No.	Ni:en	N <sub>2</sub> H <sub>4</sub> (mL)	Time (h)	Temperature (°C)
1	1:4	1	12	180
2	1:3	1	12	180
3	1:2	1	12	180
4	1:4	2	12	180
5	1:4	3	12	180
6	1:4	0.5	12	180
7	1:4	0.25	12	180
8	1:4	0.125	12	180
9	1:4	1	12	200
10	1:4	1	12	160
11	1:4	1	12	120
12	1:4	1	6	180
13	1:4	1	18	180
14				Calcination sample No.1 at 300 °C for 4 h

with ZnO [20,21]. Although NiO nanostructures have been synthesized by the hydrothermal method and the decomposition of Ni(OH)<sub>2</sub> [22], little research has been done on the optical and field emission properties of NiO nanostructures.

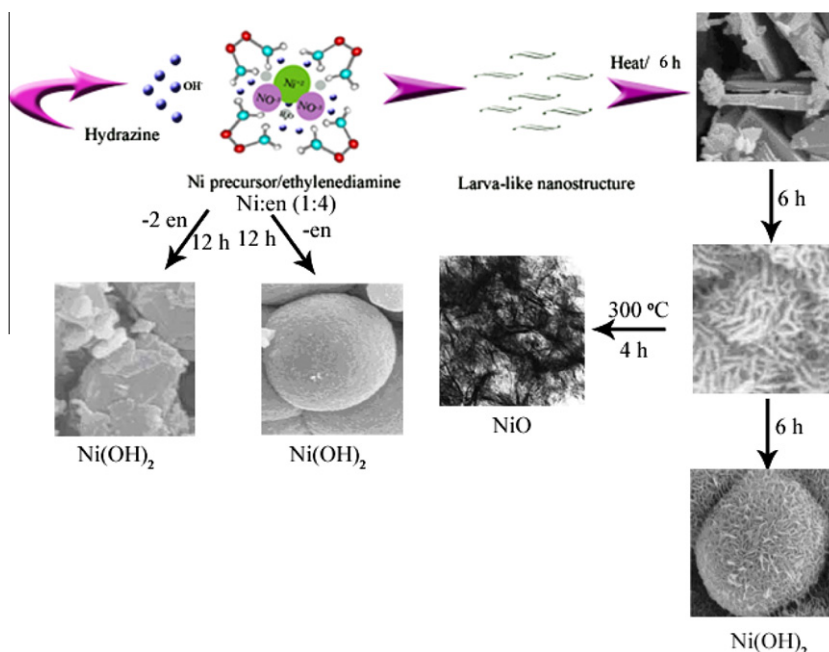
In our group, for a few years, has been interested in the synthesis of metal, metal oxide and metal sulfide nanoparticles, using new inorganic precursors and taking benefit of the tools of organometallic chemistry [23–28]. At present, the development of organometallic or inorganic compounds for the preparation of nanoparticles is of major interest [29–31]. Use of a novel compound can be helpful in opening a new way for preparing nanomaterials and in controlling the nanocrystal size, shape and distribution size.

Herein, we first report an easy method to synthesis hierarchically  $\alpha$ -Ni(OH)<sub>2</sub> nanostructures through a one-step hydrothermal synthesis with ethylene-1,2-diamine (en) and hydrazine (N<sub>2</sub>H<sub>4</sub>) as morphology-directing agents. Furthermore, NiO nanostructures were obtained by calcining the  $\alpha$ -Ni(OH)<sub>2</sub> at 300 °C under ambient pressure. The optical properties of the as-prepared samples were also investigated with the help of photoluminescence spectra.

## 2. Experimental

### 2.1. Materials and physical measurements

All reagents used were commercial products of analytical pure grade, and they were used without further purification. XRD patterns were recorded by a Rigaku D-max C III, X-ray diffractometer using Ni-filtered Cu K $\alpha$  radiation. Elemental analyses were obtained from a Carlo ERBA Model EA 1108 analyzer. The compositional analysis was done by energy dispersive X-ray (EDX, KeveX, Delta Class). Fourier transform infrared (FT-IR) spectra were recorded on a Shimadzu Varian 4300 spectrophotometer in KBr pellets. Room temperature photoluminescence (PL) was studied on an F-4500 fluorescence spectrophotometer. Thermogravimetric differential thermal analysis (TG-DTA) was carried out using a thermal gravimetric analysis instrument (Shimadzu TGA-50H) with a flow rate of 20.0 ml/min and a heating rate of 10 °C min<sup>-1</sup>. Scanning electron microscopy (SEM) images were obtained on a Philips XL-30ESEM equipped with an energy dispersive X-ray spectroscope. Transmission electron microscopy (TEM) images were obtained on



**Scheme 1.** The proposed evolution process for the preparation of Ni(OH)<sub>2</sub> and NiO nanostructures.

a Philips EM208 transmission electron microscope with an accelerating voltage of 200 kV. The magnetic measurements were carried out on a vibrating sample magnetometer (VSM) (BHV-55, Riken, Japan) at 300 K.

## 2.2. Preparation of spherical $\alpha$ -Ni(OH)<sub>2</sub> hierarchical nanostructures

In a typical procedure, Ni(NO<sub>3</sub>)<sub>2</sub>·6H<sub>2</sub>O (1 mmol), ethylene-1,2-diamine (en) (4 mmol) and hydrazine hydrate (1 mL) were first dissolved in distilled water (40 mL), and the solution was constantly stirred for 15 min at room temperature. Then the solution was transferred into a 50 mL Teflon-lined stainless steel autoclave. The autoclave was sealed and maintained at 180 °C for 12 h and then cooled to room temperature naturally. The product was filtered off, washed with distilled water and ethanol for three times, and finally dried in a vacuum oven at 60 °C for 4 h. Control experiments were carried out by adjusting the reaction temperature (120–180 °C), time of reaction (12–20 h) and the amount of N<sub>2</sub>H<sub>4</sub>·H<sub>2</sub>O (0.25–3 mL), while keeping the other reaction parameters unchanged (Table 1 and Scheme 1).

## 2.3. Thermal conversion to NiO nanostructures

The obtained products were then calcined at 300 °C for 4 h in a furnace under air to synthesize NiO. The black powder was collected for characterization.

## 3. Results and discussion

### 3.1. XRD analysis of the products

Fig. 1 presents the typical XRD patterns of the (a) spherical nickel hydroxide hierarchical nanostructures (sample No. 1), (b)

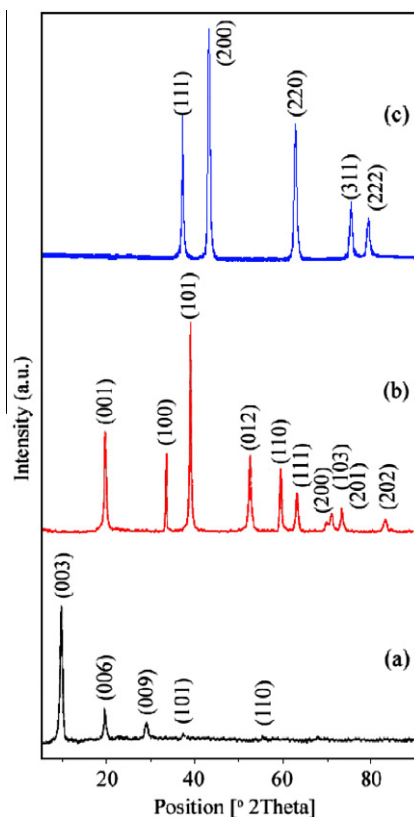


Fig. 1. XRD patterns of samples prepared under different conditions: (a) sample No. 1, (b) sample No. 13 and (c) sample No. 14.

$\beta$ -Ni(OH)<sub>2</sub> and (c) NiO. All the diffraction peaks in Fig. 1a are well indexed to a pure hexagonal  $\alpha$ -Ni(OH)<sub>2</sub> phase (JCPDS 03-0177). No diffraction peaks due to  $\beta$ -Ni(OH)<sub>2</sub> (JCPDS 14-0117) could be observed. The phases are indexed to the (003), (006), (009), (101) and (110) planes of  $\alpha$ -Ni(OH)<sub>2</sub> with well-defined peaks at

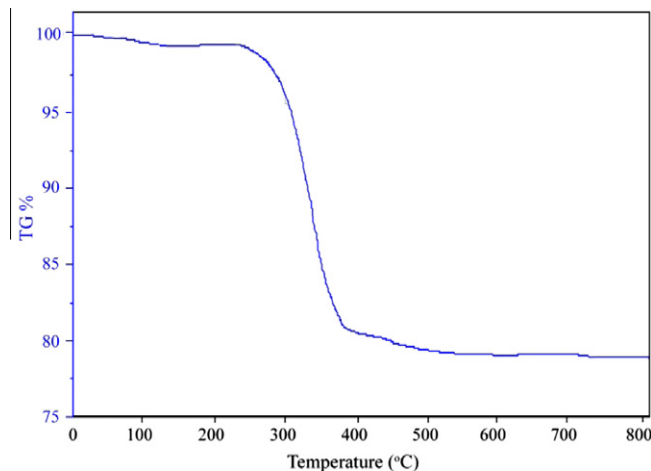


Fig. 2. Thermal gravimetric curve of  $\beta$ -Ni(OH)<sub>2</sub> (sample No. 13).

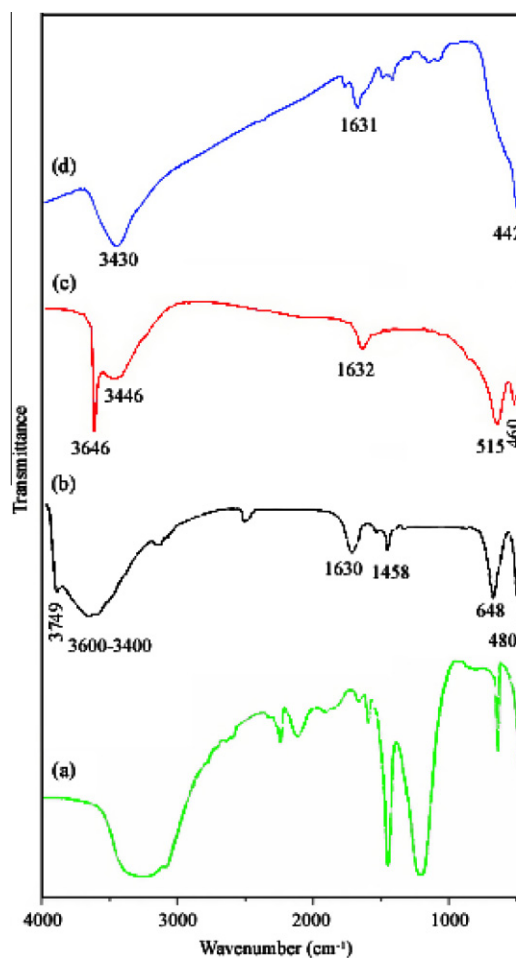


Fig. 3. FTIR spectra of samples prepared under different conditions: (a) sample No. 12 (b) sample No. 1, (c) sample No. 13 and (d) sample No. 14.

9.42, 4.73, 3.17, 2.70 and 1.55 Å. When the hydrothermal time was prolonged to 18 h (sample No. 13), a predominant well-crystalline brucite-like phase of  $\beta$ -Ni(OH)<sub>2</sub> with a hexagonal structure was formed (Fig. 1b). However, when the reaction time was prolonged to 18 h, the single phase of  $\beta$ -Ni(OH)<sub>2</sub> was obtained from the transformation of the metastable  $\alpha$ -Ni(OH)<sub>2</sub>. All of the reflection peaks of the XRD pattern of sample No. 13 (Fig. 1b) can be indexed to the pure hexagonal phase of  $\beta$ -Ni(OH)<sub>2</sub>, with lattice constants  $a = 3.128$  Å,  $c = 4.610$  Å (JCPDS 14-0117). The typical peaks at about  $d = 4.53, 2.68, 2.32, 1.75$  and  $1.56$  Å can be assigned to the (001), (100), (101), (102) and (110) planes, respectively, and also to the (111), (200), (103), (201) and (202) planes, indicating the formation of pure  $\alpha$ -Ni(OH)<sub>2</sub> [31,32]. Fig. 1c is the typical XRD pattern of NiO obtained by calcining an  $\alpha$ -Ni(OH)<sub>2</sub> sample at 400 °C for 4 h under ambient pressure. The reflection peaks in Fig. 1c can be indexed as cubic NiO phase (JCPDS 02-1216); the main diffraction peaks were observed at 37.80°, 43.44°, 62.80°, 75.21° and 79.90°. The XRD pattern of sample No. 14 confirms that the formed material is nickel oxide. All the diffraction peaks can be indexed to the pure NiO crystalline phase (space group:  $Fm\bar{3}m$ ). No obvious reflection peaks assignable to impurities can be detected in Fig. 1c, indicating the pure phase and good crystallinity of the present samples.

### 3.2. Thermal gravimetric analysis

The  $\beta$ -Ni(OH)<sub>2</sub> phase was also confirmed by thermal gravimetric analysis (TGA). The TG curve (Fig. 2) shows a weight loss of 18.9% at around 300 °C, which is equivalent to the calculated weight loss (19.4%) of one H<sub>2</sub>O molecule from  $\beta$ -Ni(OH)<sub>2</sub> to NiO. The XRD pattern of the calcined product, sample No. 14, (Fig. 1c) can be indexed to NiO (JCPDS 02-1216) [33–36].

### 3.3. FT-IR spectra of products

IR spectroscopy is a useful tool to investigate the functional groups of any organic molecule. Fig. 3a shows mixed characteristics of Ni(en)<sub>2</sub> and Ni(OH)<sub>2</sub>, (sample No. 12). According to Fig. 3a, we can conclude that 6 h are not long enough to prepare nickel hydroxide. So, for the synthesis of the pure product we must prolong the reaction time to 12 h. Fig. 3b shows the IR spectrum of the spherical nickel hydroxide hierarchical nanostructures (sample No. 1). The narrow band at 3749 cm<sup>-1</sup> was attributed to the free hydroxyl groups, and the broad band at 3600–3400 cm<sup>-1</sup> represented the hydroxyl groups and water molecules, which were extensively hydrogen bonded. The band at 1630 cm<sup>-1</sup> corresponds to the bending vibration of water molecules [37]. It can be seen from the strength of these two bands (1630 cm<sup>-1</sup> and the broad bands at 3600–3400 cm<sup>-1</sup>) that the hierarchical nanostructures of nickel hydroxide contain water molecules. The absorption around 1485 cm<sup>-1</sup> is attributed to carbonate ions [38–40] due to the open system used in the synthesis. The bands around 648 and 480 cm<sup>-1</sup> are due to the  $\delta$ OH and  $\nu$ Ni–OH vibrations, individually [41]. Fig. 3c shows a typical IR spectrum of  $\beta$ -Ni(OH)<sub>2</sub>, sample No. 13. A narrow and sharp peak at 3646 cm<sup>-1</sup> is because of the  $\nu$ O–H stretching vibration, which confirms the brucite structure of the  $\beta$ -Ni(OH)<sub>2</sub> phase. Peaks at 3446 and 1632 cm<sup>-1</sup> are assigned to the  $\nu$ (H<sub>2</sub>O) stretching vibration and  $\delta$ (H<sub>2</sub>O) bending vibration of water molecules adsorbed in the sample. The strong band at 515 cm<sup>-1</sup> corresponds to  $\delta$ O–H of hydroxyl groups. A small weak peak centered on 460 cm<sup>-1</sup> is assigned to the Ni–O stretching mode [42]. Fig. 3d shows an IR spectrum of NiO, sample No. 14. Metal oxides generally give absorption bands below 1000 cm<sup>-1</sup>, arising from interatomic vibrations. The peak at 442 cm<sup>-1</sup> in the spectrum, showing the Ni–O bond, gives clear evidence about the presence of the

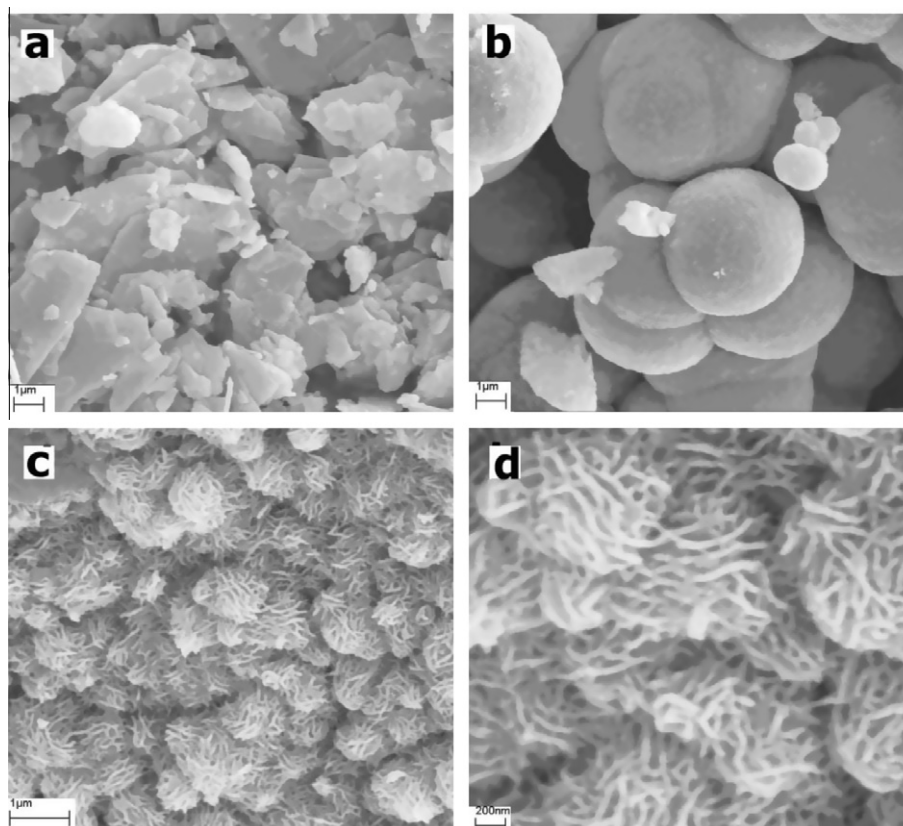


Fig. 4. SEM images of samples prepared under different conditions: (a) sample No. 3, (b) sample No. 2 and (c and d) sample No. 1.

crystalline NiO. The broad peak at  $3430\text{ cm}^{-1}$  in spectrum is representative of  $\text{H}_2\text{O}$ . Also, the H–OH bending vibration appears at  $1631\text{ cm}^{-1}$ .

### 3.4. SEM studies

#### 3.4.1. Effect of Ni:en molar ratio

Fig. 4 shows SEM images of samples prepared with different molar ratios of Ni:en. By increasing the molar ratio of Ni:en from 1:2 to 1:4, spherical nickel hydroxide hierarchical nanostructures were obtained. At a Ni:en ratio of 1:2 (see Fig. 4a) some plates with sizes bigger than  $1\text{ }\mu\text{m}$  were obtained. By increasing the concentration of ethylene diamine, microsphere nanostructures were prepared (see Fig. 4b). Ethylene diamine can play a key role in preparing spherical nanostructures. With increasing concentrations of en, to a Ni:en ratio of 1:4, larva shape nanorods were obtained (see Fig. 4c and d). The spheres are composed of a massive larva shape (or nanowall) nearly vertical to the spherical surface, which shows a high specific surface area.

#### 3.4.2. Effect of concentration of hydrazine

The formation process of hierarchical  $\text{Ni}(\text{OH})_2$  spheres was observed via different concentrations of hydrazine, by monitoring the SEM characteristics. Fig. 5 shows the SEM images of  $\text{Ni}(\text{OH})_2$  samples prepared with 0.125, 0.25, 0.5, 2 and 3 mL of hydrazine at

$180\text{ }^\circ\text{C}$  for 12 h. With 0.125 mL, (Fig. 5a),  $\text{Ni}(\text{OH})_2$  without a clear shape was formed. By increasing the amount of hydrazine to 0.25 mL,  $\text{Ni}(\text{OH})_2$  nanorods were obtained (see Fig. 5b). To prepare a spherical shape, the amount of hydrazine was increased to 0.5 mL, with this amount of hydrazine, microspheres were formed and already assembled into nanorods (Fig. 5c). Clearly, the  $\text{Ni}(\text{OH})_2$  spheres were made up of a few layers of nanorods. On increasing the concentration of hydrazine, hierarchical  $\text{Ni}(\text{OH})_2$  microspheres will be finally formed from the assembly of the nanorods, as shown in Fig. 4c and d. By increasing the hydrazine concentration to 2 and 3 mL, microspheres were formed (Fig. 5d and e). This great difference in the hierarchical morphology is just because of the concentration of hydrazine, which may be ascribed to the different nuclei and growth ratio of  $\text{Ni}(\text{OH})_2$  at the different concentrations of hydrazine. At lower concentrations (0.125, 0.25 and 0.5 mL), the nanorods can slowly be assembled into spheres with the assistance of en as a surfactant, which will further congregate into microspheres. However, under these conditions, the initial nuclei and growth ratio will be quite fast, which may destroy the assembly of the surfactant.

#### 3.4.3. Effect of reaction temperature

The hydrothermal reaction was carried out at  $120\text{ }^\circ\text{C}$  (Ni:en (1:4) and with hydrazine (1 mL) for 12 h, sample No. 11, but at this temperature no precipitate was observed. Fig. 6 shows the SEM

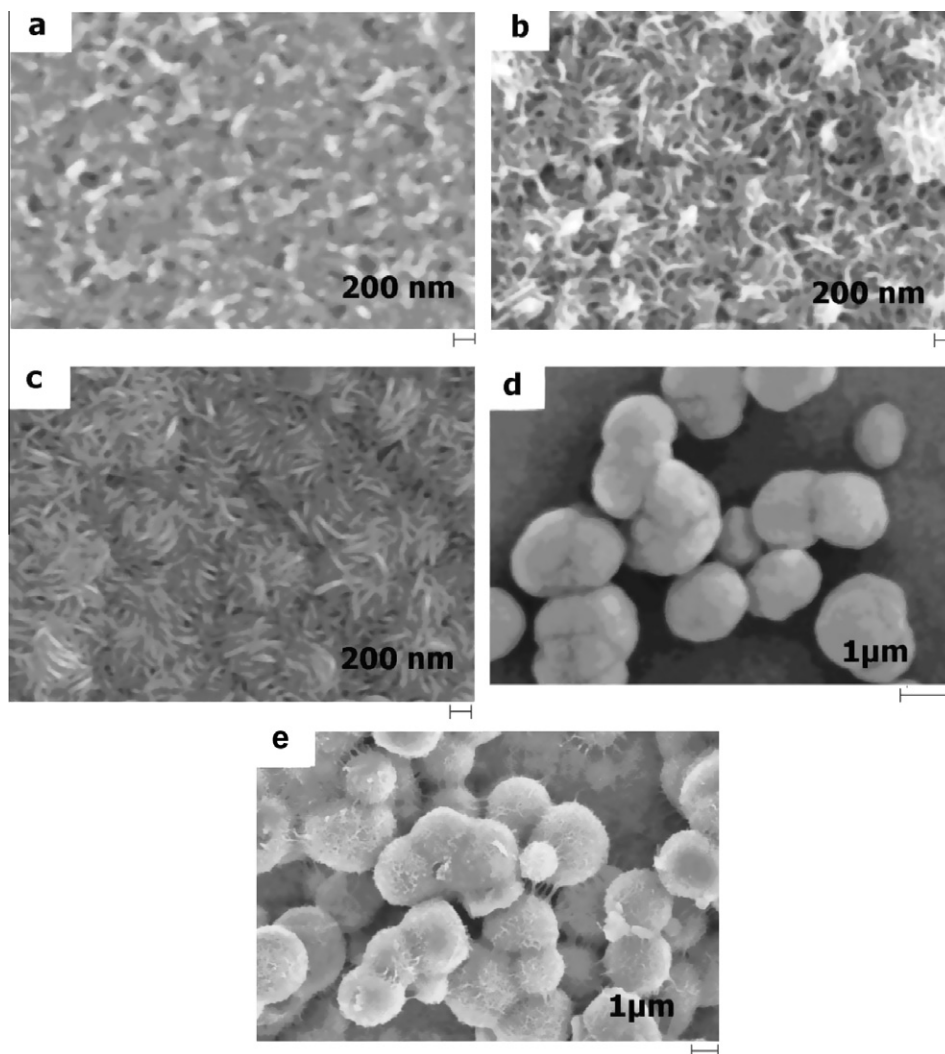


Fig. 5. SEM images of samples prepared under different conditions: (a) sample No. 8, (b) sample No. 7, (c) sample No. 6, (d) sample No. 4 and (e) sample No. 5.

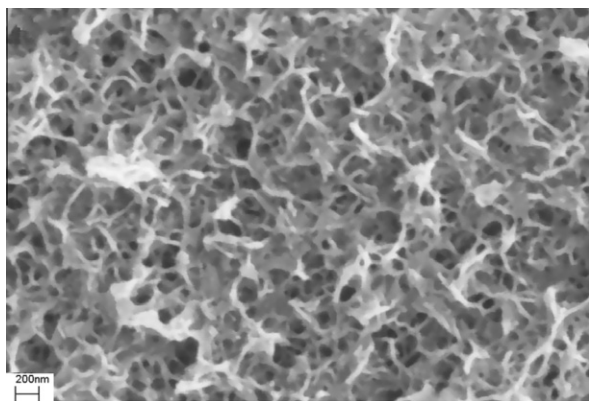


Fig. 6. SEM image of sample No. 10.

image of sample made at 160 °C which shows that the morphology is similar to sample No. 7 (see Fig. 5b).

#### 3.4.4. Effect of reaction time

In order to investigate the formation mechanism of the hierarchical  $\text{Ni}(\text{OH})_2$ , detailed time-dependent experiments were carried out at 180 °C. From the SEM images of these products, shown in Fig. 7, the morphology evolution of the hierarchical nickel hydroxide nanostructures is observed. In the middle, when the reaction time was 6 h (Fig. 7a), some blocks with some

nanosheets on their surfaces were obtained with a size of about 1  $\mu\text{m}$  and length of about 0.5  $\mu\text{m}$ . When the reaction time was increased to 8 h, the blocks gradually diminished, while nanorods gradually appeared (not shown here). Then, on prolonging the reaction time to 12 h, all the sheets disappeared and larva shape nanorods appeared in the solution, which were about 50 nm in diameter and 1  $\mu\text{m}$  in length (Fig. 4d). Looking carefully at Fig. 4d, we found that the surfaces of some nanorods were smooth. When the reaction time was 12 h, the hierarchical nanorods derived from the former smooth nanorods take shape and become the main morphology of products, as shown in Fig. 4d [2]. After prolonging the reaction time to 18 h, as shown in Fig 7b, the hierarchical nanorods become more uniform and perfect, there being no obvious variation in the diameter and length of the rods, which further demonstrates that the obtained products are not formed by the growth of additional nanorods.

#### 3.5. TEM studies

Fig. 8 demonstrates representative TEM images of the as-obtained (a)  $\alpha\text{-Ni}(\text{OH})_2$ , sample No. 1, and (b) NiO, sample No. 14. In Fig. 8a, it can be seen that the sample consists of a number of  $\alpha\text{-Ni}(\text{OH})_2$  spheres with high hierarchical structures, having an average diameter of 400 nm. These  $\alpha\text{-Ni}(\text{OH})_2$  spheres are actually constructed from a large number of nanorods. The present TEM results, to some extent, contribute to the previous reports on the synthesis of  $\alpha\text{-Ni}(\text{OH})_2$  [43]. Fig. 8b shows the TEM image of the NiO nanostructures without spherical shape, but hierarchical nanorods can be seen in Fig. 8b.

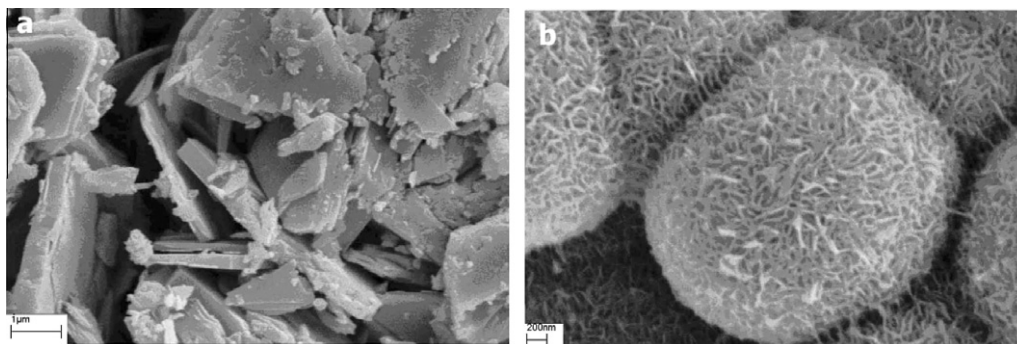


Fig. 7. SEM images of samples prepared with different reaction times: (a) sample No. 12 and (b) sample No. 13.

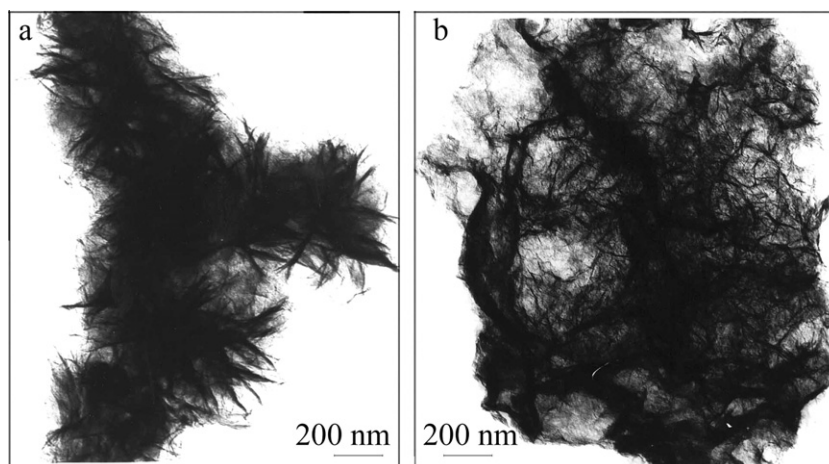


Fig. 8. TEM images of samples prepared under different conditions: (a)  $\alpha\text{-Ni}(\text{OH})_2$ , sample No. 1 and (b) NiO, sample No. 14.

### 3.6. Photoluminescence studies

Fig. 9 shows the PL spectrum of nickel oxide nanostructures, sample No. 14, excited at a wavelength of 270 nm. An emission band centered at 395.0 nm (3.17 eV) and a weak emission peak at 470 nm (2.64 eV) can be observed. As a typical transition metal element, the optical properties and carrier related phenomena in Ni compounds are governed by  $d \leftrightarrow d$  transitions present within the band gap. The nickel(II) ion has the configuration  $3s^2 3p^6 3d^8$ . This transition metal ion has six  $O^{2-}$  surrounding ions to form an elementary octahedron with octahedral symmetry. The oxygen ions crystal field splits the d electron states into  $e_g$  and  $t_{2g}$  states. [44]. According to ligand field theory, the two emission transitions

can be assigned to the  ${}^1T_{1g}(G) \rightarrow {}^3A_{2g}$  and  ${}^1T_{2g}(D) \rightarrow {}^3A_{2g}$  transitions, respectively [45]. Compared to the bulk, the photoluminescence from the NiO nanostructures is red shifted. This may be due to the wide particle size distribution and the native defects in the NiO nanostructures. No remarkable emission peak was observed in the PL spectra of  $\alpha$ -Ni(OH)<sub>2</sub> nanostructures [46].

### 3.7. Magnetic properties

The magnetic properties of Ni(OH)<sub>2</sub>, sample No. 1, and NiO, sample No. 14, nanostructures have been measured at 300 K (Fig. 10). It can be seen that Fig. 10a exhibits typical antiferromagnetism, while in Fig. 10b the NiO nanostructures present superparamagnetic behavior, although NiO bulk material is antiferromagnetic [47].

## 4. Conclusions

In summary, we have demonstrated that  $\alpha$ -Ni(OH)<sub>2</sub> and  $\beta$ -Ni(OH)<sub>2</sub> hierarchical structures aggregated by nanorods can be synthesized through the reaction of Ni(NO<sub>3</sub>)<sub>2</sub>·6H<sub>2</sub>O, en and N<sub>2</sub>H<sub>4</sub> as morphology-directing agents via an easy hydrothermal method. The formation of hierarchically Ni(OH)<sub>2</sub> nanostructures followed a self-aggregation mechanism. The key factors influencing the formation of hierarchical Ni(OH)<sub>2</sub> were monitored using SEM characterizations. The effect of the amount of hydrazine on the Ni(OH)<sub>2</sub> morphology was also investigated. NiO nanostructures assembled from nanorods were also obtained by calcination of the as-prepared  $\alpha$ -Ni(OH)<sub>2</sub> at 300 °C for 4 h in the air. Two photoluminescence emission peaks assigned to the  ${}^1T_{1g}(G) \rightarrow {}^3A_{2g}$  and  ${}^1T_{2g}(D) \rightarrow {}^3A_{2g}$  transitions of nickel(II) in oxygen coordinated octahedral sites were detected. The investigated physical properties of the  $\alpha$ -Ni(OH)<sub>2</sub> nanostructures and NiO nanostructures is very important for their applications in the future. The magnetic investigation has shown a superparamagnetic behavior for the obtained NiO nanostructures.

## Acknowledgement

The authors are grateful to the council of the University of Kashan for their unending effort to provide financial support to undertake this work.

## References

- [1] C. Xu, L. Wang, D. Zou, T. Ying, Mater. Lett. 62 (2008) 3181.
- [2] Y. Shao, J. Sun, L. Gao, J. Phys. Chem. C 113 (2009) 6566.
- [3] K. Xu, W. Ding, Mater. Lett. 62 (2008) 4437.
- [4] C. Coudun, J.F. Hochepeid, J. Phys. Chem. B 109 (2005) 6069.
- [5] X. Wang, H. Luo, P.V. Parkhutik, A.C. Millan, E. Matveeva, J. Power Sources 115 (2003) 153.
- [6] J.J. Braconniera, C. Delmas, P. Hagenmuller, Mater. Res. Bull. 17 (1982) 993.
- [7] B. Liu, X.Y. Wang, H.T. Yuan, Y.S. Zhang, D.Y. Song, Z.X. Zhou, J. Appl. Electrochem. 29 (1999) 855.
- [8] I. Zhitomirsky, J. Appl. Electrochem. 34 (2004) 235.
- [9] W.Y. Li, S.Y. Zhang, J. Chen, J. Phys. Chem. B 109 (2005) 14025.
- [10] R. Acharya, T. Subbaiah, S. Anand, R.P. Das, Mater. Chem. Phys. 81 (2003) 45.
- [11] A. Delahaye-Vidal, M. Figiarz, J. Appl. Electrochem. 17 (1987) 589.
- [12] M. Dixit, G.N. Subbanna, P.V. Kamath, J. Mater. Chem. 6 (1996) 1429.
- [13] Y.L. Zhao, J.M. Wang, H. Chen, T. Pan, J.Q. Zhang, C.N. Cao, Int. J. Hydrogen Energy 29 (2004) 889.
- [14] F. Portemer, A. Delahaye-Vidal, M. Figiarz, J. Electrochem. Soc. 139 (1992) 671.
- [15] M. Akine, N. Jongen, J. Lemaitre, H. Hofmann, J. Eur. Ceram. Soc. 18 (1998) 1559.
- [16] M. Yoshio, Y. Todorov, K. Yamato, H. Noguchi, J. Itoh, M. Okada, T. Mouri, J. Power Sources 74 (1998) 46.
- [17] B. Sheela, H. Gomathi, G.P. Rao, J. Electroanal. Chem. 394 (1995) 267.
- [18] C.B. Alcock, B.Z. Li, J.W. Fergus, L. Wang, Solid State Ionics 53 (1992) 39.
- [19] A.C. Felici, F. Lama, M. Piacentini, T. Papa, D. Debowska, A. Kisiel, A. J. Appl. Phys. 80 (1996) 6925.
- [20] D. Adler, J. Feinleib, Phys. Rev. B 2 (1970) 3112.

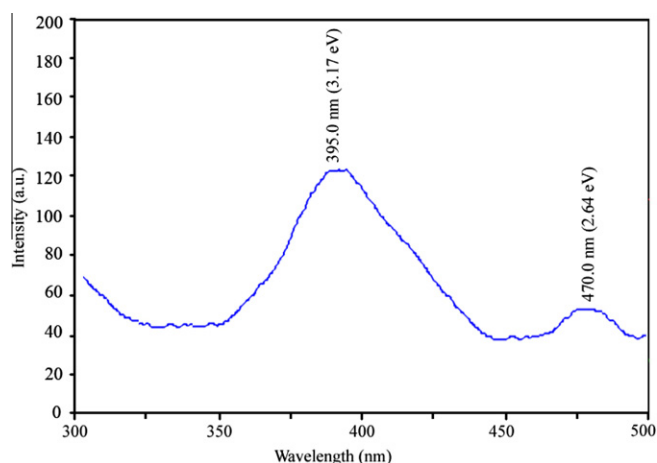


Fig. 9. PL spectrum of NiO nanostructures, sample No. 14, excited at a wavelength of 270 nm.

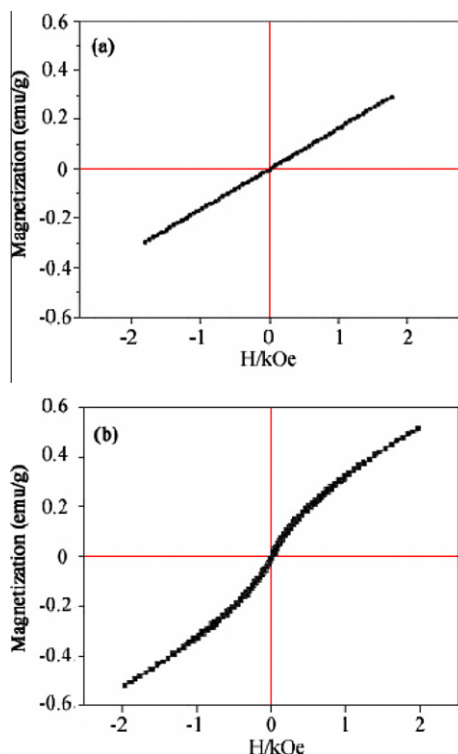


Fig. 10. The hysteresis loops of (a) Ni(OH)<sub>2</sub> (sample No. 1) and (b) NiO (sample No. 14) nanostructures at 300 K.

- [21] A. Chrissanthopoulos, S. Baskoutas, N. Bouropoulos, V. Dracopoulos, P. Pouloupoulos, S.N. Yannopoulos, *Photon. Nanostruct. Fundament. Appl.* 9 (2011) 132.
- [22] X. Wang, J.M. Song, L.S. Gao, J.Y. Jin, H.G. Zheng, Z.D. Zhang, *Nanotechnology* 16 (2005) 37.
- [23] F. Davar, M. Salavati-Niasari, Z. Fereshteh, *J. Alloys Compd.* 496 (2010) 638.
- [24] M. Salavati-Niasari, F. Davar, *Mater. Lett.* 63 (2009) 441.
- [25] M. Salavati-Niasari, M.R. Loghman-Estarki, F. Davar, *J. Alloy. Compd.* 145 (2009) 346.
- [26] M. Salavati-Niasari, N. Mir, F. Davar, *J. Alloys Compd.* 476 (2009) 908.
- [27] F. Davar, Z. Fereshteh, M. Salavati-Niasari, *J. Alloys Compd.* 476 (2009) 797.
- [28] N. Bouropoulos, G.C. Psarras, N. Moustakas, A. Chrissanthopoulos, S. Baskoutas, *Phys. Status Solidi A* 205 (2008) 2033.
- [29] F. Mohandes, F. Davar, M. Salavati-Niasari, *J. Magn. Magn. Mater.* 322 (2010) 872.
- [30] M. Salavati-Niasari, F. Mohandes, F. Davar, K. Saberyan, *Appl. Sur. Sci.* 256 (2009) 1476.
- [31] S. Baskoutas, P. Giabouranis, S.N. Yannopoulos, V. Dracopoulos, L. Toth, A. Chrissanthopoulos, N. Bouropoulos, *Thin Solid Films* 515 (2007) 8461.
- [32] D. Yang, R. Wang, M. He, J. Zhang, Z. Liu, *J. Phys. Chem. B* 109 (2005) 7654.
- [33] M. Jayalakshmi, N. Venugopal, B.R. Reddy, M.M. Rao, *J. Power Source* 150 (2005) 272.
- [34] Z.H. Liang, Y.J. Zhu, X.L. Hu, *J. Phys. Chem. B* 108 (2004) 3488.
- [35] W.K. Hu, X.P. Gao, D. Noreus, T. Burchardt, N. Nakstad, *J. Power Source* 160 (2006) 704.
- [36] H. Zhang, H. Liu, X. Cao, S. Li, C. Sun, *Mater. Chem. Phys.* 79 (2003) 37.
- [37] P. Jeevanandam, Y. Koltypin, A. Gedanken, *Nano. Lett.* 1 (2001) 263.
- [38] M. Salavati-Niasari, F. Davar, Z. Fereshteh, *J. Alloys Compd.* 494 (2010) 410.
- [39] M. Salavati-Niasari, N. Mir, F. Davar, *J. Alloys Compd.* 493 (2010) 163.
- [40] N.V. Kosova, E.T. Devyatkina, V.V. Kaichev, *J. Power Source* 174 (2007) 735.
- [41] L. Xu, Y.-S. Ding, C.-H. Chen, L. Zhao, C. Rimkus, R. Joesten, S.L. Suib, *Chem. Mater.* 20 (2008) 308.
- [42] L.-X. Yang, Y.J. Zhu, H. Tong, Z.H. Liang, L. Li, L. Zhang, *J. Solid State Chem.* 180 (2007) 2095.
- [43] X. Chen, Z. Zhang, C. Shi, X. Li, *Mater. Lett.* 62 (2008) 346.
- [44] C. Díaz-Guerra, A. Remoñá, J.A. Garcíá, J. Piqueras, *Phys. Status Solid A: Appl. Res.* 163 (1991) 497.
- [45] T. Tsuboi, W. Kleeman, *J. Phys. Condens. Mater.* 6 (1994) 8625.
- [46] Y. Qi, H. Qi, C. Lu, Y. Yang, Y. Zhao, *J. Matter. Sci.: Mater. Electron.* 20 (2009) 479.
- [47] H. Bia, S. Li, Y. Zhang, Y. Du, *J. Magn. Magn. Mater.* 277 (2004) 363.